Role of *N*-glycosylation in renal betaine transport*

Eva S. Schweikhard[1,2], Birgitta C. Burckhardt[3], Friedericke Joos[1], Cristina Fenollar-Ferrer[4.5], Lucy R. Forrest[4,5], Stephen A. Kempson[6] and Christine Ziegler[1,2*]

[1] Structural Biology Department Max Planck Institute of Biophysics, Max-von-Laue-Straße 3, 60438 Frankfurt am Main, Germany

[2] Faculty of Biology and Preclinical Medicine, Universitätsstraße 31, Regensburg, Germany

[3] Department of Systemic Physiology and Pathophysiology, University Medical Center Göttingen, Humboldtallee 23, 37073 Göttingen, Germany

[4] Computational Structural Biology Group, Max Planck Institute of Biophysics, Max-von-Laue-Strasse 3, 60438 Frankfurt am Main, Germany

[5] Current address: Computational Structural Biology Section, Porter Neuroscience Research Center, National Institutes of Neurological Disorders and Stroke, National Institutes of Health, Bethesda MD 20892, USA

[6] Department of Cellular and Integrative Physiology, Indiana University School of Medicine, Indianapolis

*Running Title: *Role of N-glycosylation in BGT-1*

[‡]To whom correspondence should be addressed: Christine Ziegler, Max Planck Institute of Biophysics, Department of Structural Biology, Max-von-Laue-Str. 3, D-60438, Frankfurt am Main, Germany, Tel.: (+49) 69 6303-3054; Fax: (+49) 69 6303-3002; E-mail: Christine.Ziegler@biophys.mpg.de

This is the author's manuscript of the article published in final edited form as:

Schweikhard, E. S., Burckhardt, B. C., Joos, F., Fenollar-Ferrer, C., Forrest, L. R., Kempson, S. A., & Ziegler, C. (2015). Role of N-glycosylation in renal betaine transport. Biochemical Journal, BJ20131031. http://doi.org/10.1042/BJ20131031

ABSTRACT

The osmolyte and folding chaperone betaine is transported by the renal Na^+-coupled GABA symporter BGT-1, a member of the SLC6 family. Under hypertonic conditions, the transcription, translation and plasma membrane insertion of BGT-1 in kidney cells are significantly increased, resulting in elevated betaine and GABA transport. Re-establishing isotonicity involves plasma membrane depletion of BGT-1. The molecular mechanism of the regulated plasma membrane insertion of BGT-1 during changes in osmotic stress is unknown. Here we reveal a link between regulated plasma membrane insertion and *N*-glycosylation. Based on homology modelling we identified two sites (N171 and N183) in the extracellular loop 2 (EL2) of BGT-1, which were investigated with respect to trafficking, insertion, and transport by immunogold-labelling, electron microscopy, mutagenesis, and two-electrode voltage clamp measurements in *Xenopus laevis* oocytes, and uptake of radiolabelled substrate into MDCK and HEK cells. Trafficking and plasma membrane insertion of BGT-1 was clearly promoted by *N*-glycosylation in both oocytes and MDCK cells. Moreover, association with *N*-glycans at N171 and N183 contributed equally to protein activity and substrate affinity. Substitution of N171 and N183 by aspartate individually caused no loss of BGT-1 activity, while the double mutant was inactive, suggesting that *N*-glycosylation of at least one of the sites is required for function. Substitution by alanine or valine at either site caused a dramatic loss in transport activity. Furthermore, in MDCK cells plasma membrane insertion of N183D was no longer regulated by osmotic stress, highlighting the impact of *N*-glycosylation in regulation of this SLC6 transporter.

Keywords: GABA transport, kidney, NSS/SLC6 family, osmotic stress response, regulation, subcellular distribution

INTRODUCTION

Secondary active transporters play important roles in maintaining vital functions in mammalian kidneys [1, 2], which constantly encounter major changes in osmolality during urinary concentration [3]. The renal hydration state is adjusted by accumulation of several osmolytes, e.g., betaine, taurine, sorbitol, glycerophosphorylcholine (GPC) and *myo*-inositol [4]. For example, the *myo*-inositol transporter SMIT (SLC5A3) and the betaine/γ-aminobutyric acid (GABA) transporter BGT1 (alias GAT2, SLC6A12) accomplish cellular accumulation of *myo*-inostol and betaine, respectively, and thus contribute to cell volume regulation in the kidneys. Moreover, betaine-mediated volume regulation prevents severe dysfunction of the kidneys and the central nervous system [5-7] and counteracts the destabilizing action of urea on protein structures in renal cells [8, 9].

BGT-1, which belongs to the osmolyte branch of the human Neurotransmitter Sodium Symporter (NSS) or Solute Carrier 6 (SLC6) family [10] is also found in the brain and in the liver [11, 12]. BGT-1 mediates the transport of the neurotransmitter GABA, however with a lower affinity compared to other GABA transporters [10]. Both betaine and GABA transport are chloride-dependent and coupled to the transport of 3 sodium ions [13, 14], which might be required to provide in the kidneys a sufficient driving force in order to achieve an intracellular renal medullary cell betaine concentration of around 100 mM [15, 16]. During hypertonicity, both *bgt-1* transcription and BGT-1 insertion into the basolateral plasma membranes are increased so that transport of betaine is up-regulated in Madin-Darby-Canine kidney cells (MDCK) [17]. Like BGT-1, SMIT1 expression is rapidly stimulated during hypertonicity, leading to increased *myo*-inositol uptake from the extracellular space [18].

To date, the genomic regulation of BGT-1 and the other organic osmolyte transporters SMIT1 and TauT involve the transcription factor tonicity enhancer binding protein (TonEBP) [19-21]. During hypertonicity TonEBP is activated and binds to tonicity responsive enhancers (TonE) on the BGT-1 promoter region thereby inducing its transcription [19]. Upon hypertonic conditions binding of TonEBP to the promotor region of osmosensitive genes was therefore considered to be a general mechanism to protect cells from shrinkage. Furthermore, Klaus et al could show that the cell volume-sensitive protein kinase SGK1 modulates SMIT1 function by increasing its plasma membrane abundance without affecting transport kinetics [22].

Beyond that, the molecular mechanisms of stress sensing and regulation of plasma membrane insertion of BGT-1 are unknown.

Controlled folding by *N*-glycosylation might be one regulatory mechanism, as *N*-glycans are reported to affect targeting and functional insertion to the plasma membrane in several proteins [23, 24]. The role of *N*-glycosylation sites in the second extracellular loop (EL2, Fig. 1A) of SLC6 transporters has been widely discussed [25-30]. EL2 connects transmembrane domains (TMs) 3 and 4 (Fig. 1B). In NSS/SLC6 transporters TM3 is not directly involved in substrate or sodium ion binding. However, structural data on bacterial homologues have revealed that together with TM8 that harbours residues contributing to the Na2 sodium ion binding site TM3 undergoes conformational changes during the transport cycle [31]. *N*-glycosylation sites in EL2 are not conserved across all members of the SLC6 family (Fig. 1A) consistent with the fact that individual SLC6 transporters seem to be differently affected by *N*-glycosylation [25-28, 30]. For instance, mutations of two of the three *N*-glycosylation sites in the GABA transporter GAT1 expressed in *Xenopus* oocytes yielded a reduction of turnover

rates and significant changes in affinity to sodium [27], while the human dopamine transporter, DAT, showed reduced inhibitor affinity when *N*-glycosylation was altered [26].

Here, we present biochemical and functional data describing the role of the two predicted *N*-glycosylation sites in canine BGT-1. We observe that functional BGT-1 requires at least one of these sites (either N171 or N183) to be associated with *N*-glycans, while in the other site (either N171 or N183) the effect of *N*-glycosylation has to be mimicked by an aspartate, at a minimum. Our data further suggest that the increased plasma membrane insertion of BGT-1 upon a hyperosmotic shock requires the association of N183 with *N*-glycans.

MATERIALS AND METHODS

DNA constructs and cRNA synthesis for *Xenopus* oocytes

Wild type (WT) cDNA of canine BGT-1 was cloned into pTLN Vector (gift from Prof. Bamberg, Department of Biophysical Chemistry, Max Planck Institute of Biophysics, Frankfurt) with XbaI and XhoI restriction sites.

Site directed mutagenesis

The QuikChange™ kit (Stratagene, Santa Clara, CA), in combination with *Pfu* Turbo DNA polymerase, was used for the insertion of the desired mutations, N171D, N183D and NN171/183DD in the *pTLN-BGT-1* plasmid. All the plasmids were fully sequenced and the specific mutations were confirmed. WT and mutants of *pTLN-BGT-1* were linearized using *MluI*. Linearized DNA was further purified with High Pure PCR Product Purification Kit (Roche, Mannheim, Germany) and concentrated up to 0.17 µg/µl for *in vitro* RNA-synthesis using the mMESSAGE mMACHINE SP6 Kit (life technologies, Ambion, Grand Island, NY).

Expression and two-electrode voltage clamp analysis of WT and mutants in *Xenopus laevis* oocytes

A standard oocyte Ringer solution (ORi) was used for oocyte preparation, storage, and for the electrophysiology measurements. ORi contained (in mM): 110 NaCl, 3 KCl, 2 $CaCl_2$, 5 HEPES/Tris, adjusted to pH 7.5. GABA was added to ORi in the following concentrations: 0.01; 0.025; 0.05; 0.1, 0.25; 0.5, and 1 mM, adjusted to pH 7.5. All chemicals were purchased from Sigma-Aldrich (Taufkirchen, Germany).

Oocyte preparation and storage

Stage V and VI oocytes from *Xenopus laevis* (Nasco, Fort Atkinson, WI) were separated by an overnight treatment with collagenase (Typ CLS II, Biochrom, Berlin, Germany), subsequent washings in calcium-free ORi and maintained at 16 – 18 °C in ORi containing again a calcium concentration of 2 mM. One day after removal from the frog, oocytes were injected either with 23 nl 1mg/2ml tunicamycin (AppliChem, Darmstadt, Germany) solved in ORi or 23 nl ORi alone approximately 60 min prior to injection of cRNA coding either for the wildtype BGT-1 or the mutants. An equivalent amount of ORi was injected as a control (mocks). Tunicamycin inhibits enzymes involved in the first steps of *N*-linked glycoprotein synthesis in the endoplasmic reticulum (ER). Oocytes were maintained at 16–18 °C in ORi supplemented with 50 µM gentamycin and 2.5 mM sodium pyruvate, daily washings and discarding of damaged oocytes.

Electrophysiologic analysis

These studies were carried out 3–4 days after cRNA and tunicamycin injection at room temperature. Oocytes were placed into a 0.5 ml chamber on the stage of a microscope and impaled under direct view with borosilicate glass microelectrodes filled with 3 M KCl (BioMedical Instruments, Zöllnitz, Germany). Current recordings at –60 mV were performed using a two-electrode voltage clamp device (OC725A, Warner, Hambden, CT) in the voltage clamp mode.

Statistics and calculations

Data are provided as means ± SEM. Paired Student's t-test was used to show statistically significant difference of the GABA-associated currents in the absence and presence of

PNGaseF. Statistical significance was set at $p<0.05$ (*). Michaelis-Menten constants (K_M) for GABA in the absence and presence of tunicamycin were determined by SigmaPlot software (Systat Software, Point Richmond, CA) using the Michaelis-Menten equation $I = I_{max} \cdot [S]/(K_M + [S])$, where I is the current, I_{max} is the maximum current observed at saturating substrate concentrations, K_M is the substrate concentration at half-maximal current, and S is the substrate concentration.

Membrane preparation

Preparation of membranes was carried out as described previously [32]. The lysates were separated on 12.5 % SDS-PAGE and then electro-transferred onto PVDF-membranes which were previously activated by methanol. The membrane was blocked with 5 % milk powder for 1h at room temperature and then incubated over night at 4 °C with affinity-purified rabbit polyclonal antibody to dog BGT-1 (Proteintech Group, Chicago, IL), diluted 1:1000 in 0.5 % milk powder, followed by a 2 h incubation with affinity-purified polyclonal antibody to rabbit coupled to alkaline phosphatase, diluted 1:1000 in 0.5 % milk powder.

Fractionation of oocytes membranes

Fractionation was carried out according to the protocol from Broer [32] with minor changes. Briefly, 80 oocytes of WT, 100 oocytes of WT^{+Tun} and WT^{+P} and 150 oocytes of NN171/183DD were homogenized in 1 ml, 1.5 ml and 2 ml "homogenization buffer 2" (in mM): 320 Sucrose, 50 Tris, 1 EDTA, 1 Pefabloc, adjusted to pH 7.5, respectively by pipetting up and down. The suspension was centrifuged twice at 1000*g for 10 min at 4 °C. The supernatants were transferred on a sucrose gradient: 2 ml [2M], 3.2 ml [1.3 M], 3.2 ml [1 M], 2 ml [0.6 M] and centrifuged in a SW40 rotor (Beckman Coulter, Krefeld, Germany) at 40,000 rpm for 4 h at 4 °C. Sucrose solutions were prepared in "TE-buffer" (in mM): 50 Tris, 1 EDTA, 5 $MgCl_2$, adjusted pH 7.5). 1 ml fractions were collected from the bottom, diluted 4-fold with 150 mM Sucrose in "TE-buffer" and centrifuged at 50,000 rpm in a Ti70 (Beckman) rotor for 2 h at 4 °C. Pellets were resuspended in 15 µl SDS-PAGE sample buffer for electrophoresis and Western blotting as described above. The rough ER (rER) is detected in fractions 2-3, the plasma membrane (PM) in fraction 5 and the trans-Golgi network (TGN) in fractions 9-10 [33].

Fixation and determination of cell surface expression by immunogold-labeling

Post-embedding immunogold labeling and electron microscopy followed the method of Haase[34] and Lörinczi et al[35], except that *Xenopus laevis* oocytes were treated with 4 % paraformaldehyde (PFA) in ORi solution pH 7.5, for 3 hours. The antibodies used for immunogold labeling of thin sections were the primary anti-BGT-1 (dog) (Proteintech Group, Chicago, IL, USA) and the second against rabbit coupled to gold particles (diameters 10-12 nm, both diluted 1:100 in PBS supplemented with 0.1 % BSA) for visualization.

Cell culture of MDCK and HEK cells and [^{3}H]GABA transport assays

MDCK cells (CCL-34, from American Type Culture Collection (Rockville, MD)) and HEK cells were used as described previously [36, 37]. Na^+- dependent [^{3}H]GABA (Moravek Biochemicals and Radiochemicals, Brea, CA) uptake was determined in 6-well plates according to [37]. Enzymatic deglycosylation with PNGase F was carried out by adding 10 Units/ml PNGase F (New England BioLabs, Ipswich, MA), an enzyme catalysing the complete removal of *N*-glycan chains from glycoproteins to the isotonic and hypertonic sodium medium respectively incubating for 6 hours at 37 °C prior measuring. MDCK cells were transiently transfected using GeneJammer (Stratagene, Santa Clara, CA, USA) according to the manufactors instructions. GraphPad Prism version 5.0c for Mac OS X, GraphPad software [38] was used for the kinetic constants which were derived by Michaelis-Menten curve fitting of the uptakes rates versus the substrate concentration. Data are means ±

SD of at least three separate experiments. In each transport experiment, the mean value was derived from triplicate determinations. Where appropriate, different groups were compared by ANOVA and Tukey's test for multiple comparisons, using GraphPad Prism version 5.0c for Mac OS X, GraphPad software [38]. A probability of $P < 0.05$ was considered statistically significant.

Fluorescence microscopy and Western blotting

Fluorescence microscopy and Western blotting of cell lysates was carried out according to [36].

Sequence alignment of EL2 and structural modelling of human BGT-1

The transmembrane domain of BGT-1 in an outward-occluded state was modelled using the X-ray structure of dmDAT as template (PDB entry 4M48). The sequence alignment of human and dog BGT-1, human GAT1, GAT2, GAT3, human TauT, human DAT, and the dmDAT construct used for X-ray crystallography, was obtained using T-Coffee v10 [39]. The alignment was manually refined in EL2, residues (160-178), to match the predicted *N*-glycosylation sites (Fig. 1A). The sequence identity between dmDAT and human BGT-1 in this alignment is 47.2 %. Based on this alignment, a set of 2000 structural models of human BGT-1 was generated using Modeller 9v2 [40] and the selected model was that with the best agreement with the Ramachandran plot according to Procheck [41] taken from the ten models with the lowest Modeller molpdf scores. The final BGT-1 model has zero residues in disallowed regions of the Ramachandran plot, and just one (R413) in a generously allowed region; R413 is located in a loop segment.

RESULTS

Implications of *N*-glycosylation in BGT-1 from homology modelling

A multiple-sequence alignment of representative mammalian NSS transporters (SLC6 family) reveals at least six distinct *N*-glycosylation motifs in EL2, which we label according to their positions from 1 (N-terminal) to 6 (C-terminal) (Fig. 1A). These sites are not simultaneously conserved in all members of this family nor are there any obvious pattern in distribution or number of sites for different branches of the NSS family (Fig. 1A). Focussing on the osmolyte branch, BGT-1 is predicted to have two *N*-glycosylation sites [13], 3 and 6, while the EL2 of other GABA transporters (GAT1, GAT2 and GAT3) includes the same sites 3 and 6, in addition to either site 4 or site 5. The taurine transporter TauT, which contains sites 3 and 6, also shares site 1 with the human dopamine transporter hDAT.

In order to identify the positions of the *N*-glycosylation sites in EL2 in three dimensions, we constructed a homology model of human BGT-1 (Fig. 1B, C), based on the recently published structure of the *Drosophila melanogaster* dopamine transporter (dmDAT) [42]. This structure revealed important information on the mechanism of antidepressant binding and substrate inhibition. Although EL2 is truncated by 42 residues (Δ164-206) in dmDAT the structure shows important parts of the architecture of EL2 including the second *N*-glycosylation site at N183. Therefore, EL2 in BGT-1 could be modelled using the dmDAT structure as template. In fact, only nine residues (Phe169-Val178) in BGT-1 have no template in dmDAT (Fig. 1). The remaining nine residues of BGT-1 were modelled using Modeller v9.2 [40]. In the resulting model, EL2 covers a large area of the extracellular surface of BGT-1, suggesting an interaction with EL4. While N183 is in close proximity to a well-ordered helical segment, N171 is located in the long segment of EL2 that lacks notable secondary structure (Fig. 1C), suggesting that *N*-glycan association may have different effects at each of these locations. To investigate whether these sites are indeed functional distinguishable, we carried out a systematic study of the roles of both predicted *N*-glycosylation sites in transport and regulation of BGT-1.

Regulation of BGT-1 mediated GABA transport in *Xenopus laevis* oocytes

We performed localization and transport measurements of chemically, enzymatically and/or by mutagenesis de-glycosylated canine BGT-1 in *Xenopus laevis* oocytes. This *in vivo* system was chosen to allow our results to be compared directly to those of other NSS transporters [25-30] as it is known that the transcription and translation machineries affect transporter properties significantly. However, *Xenopus laevis* oocytes did not survive hypertonic conditions compared to those leading to regulated plasma membrane insertion observed in MDCK cells.

This became obvious when comparing the GABA induced-currents measured under hypertonic conditions relative to those under isotonic conditions. Oocytes were superfused with 10 mM GABA (Fig. 2, black bar, 10 mM GABA), which led to inward currents in oocytes expressing BGT-1 (Fig. 2B), but not in water-injected control oocytes (Fig. 2A). After recovery from the effects of GABA, already hypertonic conditions (455 mOsM, Fig. 2, black bar, + 220 mM Sucrose) led to inward currents not only in BGT-1-expressing oocytes (Fig. 2 B) but also in water-injected control oocytes (Fig. 2A) and subsequently no GABA-mediated currents in BGT-1-expressing oocytes were observed (Fig. 2B, black bars, + 220 mM Sucrose and 10 mM GABA. Most of the oocytes did not survive long-term exposure (24 hours) to hypertonic conditions and therefore no osmotic-stress regulated insertion could be detected. In the following, therefore, the role of *N*-glycosylation of BGT-1 expressed in oocytes was investigated exclusively under isotonic (ORi, 235 mOsM) conditions, and the data are discussed only in the context of trafficking and transport, not in the context of

regulation. The regulatory role of *N*-glycosylation was considered using measurements performed in MDCK cells (see below).

Trafficking and localization of glycosylated and de-glycosylated BGT-1 in *Xenopus laevis* oocytes

We investigated the impact of *N*-glycosylation on the subcellular distribution of BGT-1 in oocytes under isotonic conditions (235 mOsM), focusing on the rough ER (rER), the trans-Golgi network (TGN), and the plasma membrane (PM) by Western Blot. Although the accuracy of a Western Blot does not allow for a quantitative analysis, the changes in intensity for similar oocyte number (~150 oocytes) are strong enough for a semi-quantitative statement. After 3 days expression, *N*-glycosylated BGT-1 is detected at ~70 kDa on the Western blot (Fig. 2C, WT) and appears to be similarly distributed in all three compartments. Nevertheless, the major fraction is found in the plasma membrane (Fig. 2C, WT, PM). The stability and abundance of plasma membrane-inserted BGT-1 was determined after enzymatically removing any surface-exposed *N*-glycans by applying PNGase F to the extracellular solution. The loss of *N*-glycans after plasma membrane insertion did not affect the amount of BGT-1 found in the rER (Fig. 2D, WT^{+P}, rER), but led to a slight increase in the TGN fraction (Fig. 2D, WT^{+P}, TGN). The de-glycosylated BGT-1 isoform (~60 kDa) is still observed in the plasma membrane without any apparent degradation (Fig. 2D, WT^{+P}, PM), implying that the BGT-1 fraction in the plasma membrane is stable without *N*-glycans, although a partial depletion and internalization is caused by their removal.

Mutagenesis of *N*-glycosylation sites in BGT-1

Treatment of oocytes with PNGase F reveals the de-glycosylated BGT-1-WT form at ~60 kDa (Fig. 3A, WT, +) and a fully glycosylated form at ~70 kDa on the Western blot in the absence of PNGase F (Fig. 3A, WT). It seems that *N*-glycosylation is less efficient in oocytes accounting for the remaining fraction of de-glycosylated WT protein.

Putative *N*-glycosylation sites were modified by replacing asparagine residues with aspartate, alanine or valine, either individually (N171D, N183D, N171A, N171V, N183V), or in combination (NN171/183DD). When substituted by aspartate individually (N171D, N183D), a form of BGT-1 is still observed at the same molecular weight as the WT, whereas the alanine mutant (N171A) and two valine mutants (N171V, N183V) all run at lower molecular weight (Fig. 3A). N171D and N183D show a similar band shift to the WT after PNGase F treatment (Fig. 3A; N171D, N183D, +). Within the accuracy limit of the method it appears that a similar amount of *N*-glycans is attached to the remaining site as in the WT. For N183D, the glycosylated form is expressed to a lesser extent than that of WT and N171D. The double mutant, NN171/183DD, does not change electrophoretic mobility upon PNGase F treatment (Fig. 3A, NNDD, +) representing a fully un-glycosylated form of BGT-1. Both N171A and N171V show band shifts upon PNGase F treatment (Fig. 3A; N171A, +; N171V, +) confirming partial *N*-glycosylation. These two mutations (N171A, N171V) seem to alter the architecture of EL2 in a way that *N*-glycosylation of the remaining N183 is affected as shown by the lower molecular weight prior to PNGase F treatment. N183V behaves similar to the double mutant (NN171/183DD) and does not show a band shift upon PNGase F treatment (Fig. 3A, N183V, +) suggesting that N171 is completely inaccessible without *N*-glycosylation of N183 or the mimicking effect of *N*-glycosylation (via aspartate) at this position.

NN171/183DD is enriched in the rER and undergoes significant degradation in the TGN (Fig. 3B, arrow), perhaps due to a slower targeting to the plasma membrane and mis-folding. Cell surface expression was also assayed by immunogold-labelling of thin-sectioned *Xenopus* oocytes using a BGT-1 specific antibody (Fig. 3C, WT, 30 ± 5 gold-labeled BGT-1 molecules). Judged from the electron micrographs of thin sections the amount of N171D (21 ± 3), N183D (15 ± 2), and NN171/183DD (9 ± 1) inserted into the plasma membrane is slightly reduced, while it is significantly reduced for the double mutant (Fig. 3C,

NN171/183DD). The remaining fraction of NN171/183DD in the plasma membrane does not show degradation (Fig. 3B, PM). The reduced plasma membrane localization might reflect a disabling effect on plasma membrane targeting due to the NN171/183DD double mutation.

We conclude that for proper folding to occur, only one of the sites has to be glycosylated, as long as the remaining site is replaced by aspartate. The amount of BGT-1 trafficked to and inserted into the plasma membrane, however, depends on the presence of *N*-glycans at N183 indicated by the difference in expression levels for N171D and N183D.

GABA transport by BGT-1 and mutants in *Xenopus laevis* oocytes

Functional analysis of *N*-glycosylated and de-glycosylated forms of BGT-1 was carried out. GABA transport by BGT-1-WT and mutants was investigated by two-electrode voltage clamp. Apparent K_M-values were determined at a holding potential of -60 mV (Table 1). The K_M of BGT-1-WT for its substrate GABA was 11.7 ± 0.4 µM, which is in good agreement with a previous report [14]. N183D exhibited an apparent K_M value of 9.5 ± 1.2 µM for GABA, which is very close to that of BGT-1-WT. The maximal inducible current of N183D is reduced by a factor of 2 relative to WT, reflecting the lower protein concentration in the plasma membrane. NN171/183DD substrate-associated currents were below detection limits (Table 1). Interestingly, the *N*-glycosylated N171D mutant has a significantly (five-fold) higher GABA affinity even than BGT-1-WT (Table 1, N171D).

The GABA-induced currents of BGT-1-WT were reduced by 80 % at -60 mV when *N*-glycosylation was suppressed by tunicamycin (Table 1, BGT-1-WT^{+Tun}). The apparent K_M-value also increased nearly 20-fold (Table 1, BGT-1-WT^{+Tun}). Due to the apoptotic side effects of tunicamycin on all cellular components, these measurements have to be considered with caution. Indeed, compared to *N*-glycosylated BGT-1-WT only a threefold reduction in the apparent K_M for GABA was observed when *N*-glycans were removed by PNGase F after the protein was inserted into the plasma membrane (Table 1, BGT-1-WT^{+P}). Therefore, either chemical or enzymatic removal of *N*-glycans of BGT-1-WT decreases the affinity of BGT-1 for GABA and decreases GABA transport rate, while substitution of the *N*-glycosylation sites by negatively charged residues does not alter affinity and transport kinetics significantly. However, there might be also the possibility that *N*-glycosylation is indirectly affecting BGT-1 via the action of glycosylated ancillary proteins, although to date there is no indication for any interaction of BGT-1 once inserted in the plasma membrane. In addition, our *in vitro* studies in membrane vesicles (data not shown) have not indicated the necessity of additional interaction partners to facilitate transport. Substitution by either alanine or valine dramatically decreases substrate affinity (Table 1, N171A, N171V, N183V). Association with *N*-glycans at N183 appears not to be crucial as long as the site is mimicked by aspartate considering the nearly identical affinities of WT and N183D mutant (Table 1). Interestingly, the substitution of N171 by aspartate results in a significant increase in substrate affinity (Table 1). In summary, the effect on transport of *N*-glycan association at the two putative *N*-glycosylation sites is the opposite of that observed for plasma membrane insertion, i.e., *N*-glycan association to N183 is important for insertion whereas association to N171 determines transport properties.

Role of *N*-glycosylation in BGT-1 expressed in MDCK cells

Given that *N*-glycosylation of BGT-1 at N183 is important for plasma membrane insertion, we asked whether osmotic-stress-regulated insertion is also affected. Osmotic stress regulation of membrane insertion can only be observed in MDCK cells, and therefore, we repeated the key experiments performed in oocytes in MDCK cells. MDCK cells contain endogenous BGT-1 [36]. Total *N*-glycosylation of N171 (site 3, Fig. 1) and N183 (site 6, Fig. 1) were investigated both for the endogenous form (Fig. 4A) as well as for BGT-1 fused with a N-terminal 27 kDa EGFP-tag and expressed in addition to the endogenous form (Fig. 4B). Unlike oocytes, MDCK cells were able to survive hypertonic conditions and therefore BGT-1

plasma membrane insertion was induced in hypertonic medium (500 mOsM) (Fig. 4C,D, Hyp) to up-regulate substrate transport [36]. Endogenous BGT-1 shows an electrophoretic mobility of about 90 kDa on the Western blot (Fig. 4A), while the PNGase F treated cells reveal de-glycosylated endogenous protein running at ~55 kDa (Fig. 4A, WT_{end}^{+P}). The *N*-glycans in MDCK cells seem to be more complex (larger) compared to the *N*-glycans in oocytes. The de-glycosylated EGFP-tagged BGT-1 was detected at a molecular weight of ~90 kDa accounting for the molecular weight of the 27 kDa EGFP tag, while the glycosylated form runs at ~120 kDa (Fig. 4B). This corresponds to a comparable shift of ~40 ± 5 kDa from glycosylated to de-glycosylated both for endogenous and EGFP-tagged BGT-1 in MDCK cells (Fig. 4A).

In contrast to oocytes, which seem to withstand the apoptotic action of tunicamycin to some extent, MDCK cells were detrimentally affected by tunicamycin, especially under hyperosmotic conditions. Consequently, to assess the effect of *N*-glycan association on osmo-regulated insertion and withdrawing of *N*-glycan-depleted BGT-1 from the plasma membrane of MDCK cells, we treated them with PNGase F (Fig. 4A,B,$^{+P}$ and Fig. 4D, Hyp^{+P}), but not with tunicamycin. After enzymatic removal of the *N*-glycans, de-glycosylated BGT-1 remains mainly in the plasma membrane (Fig. 4D, Hyp^{+P}), suggesting that removal of *N*-glycans does not trigger depletion of plasma membrane-inserted BGT-1. That is, similar to the observation in oocytes, the removal of *N*-glycans from BGT-1 after insertion into the plasma membrane of MDCK cells does not seem to affect the amount and stability of the protein in the plasma membrane. However, when PNGase F treated MDCK cells were exposed to isotonic medium after a hyperosmotic shock, de-glycosylated BGT-1 remained mainly in the plasma membrane (Fig. 4E, $Hyp^{+P}_{recovery}$), while glycosylated BGT-1-WT is directly depleted from the plasma membrane after switching from hyperosmotic conditions to isotonic conditions (Fig. 4E, $Hyp_{recovery}$). This result is the first indication that *N*-glycosylation of BGT-1 in MDCK cells is involved in regulated plasma membrane depletion.

N183D prevents regulation in MDCK cells

Firstly the effect of *N*-glycosylation on transport was investigated in MDCK cells by measuring [^{3}H]GABA uptake by endogenous BGT-1 and K_M-values were determined (Fig. 5). The affinity for GABA was 41.6 ± 23.7 (Table 2). After PNGase F treatment (Fig. 5, open symbols), the apparent K_M-values increased by a factor of 1.2 (Table 2, BGT-1-WT^{+P}) indicating a smaller effect of *N*-glycosylation on affinity than observed in oocytes (Table 1, WT, WT^{+P}; K_M values increased by a factor of 2.5). The transport rates were reduced by a factor of 2 by PNGase F treatment (Table 2, BGT-1-WT^{+P}), showing a similar trend to the reduction in maximal inducible currents measured in oocytes (Table 1). As MDCK cells express BGT-1 WT endogenously, mutants were measured in HEK cells. Transport kinetics of both Asp mutants (N171D, N183D) (Table 2) further supports the localization studies observed for these two mutants in MDCK cells under iso- and hypertonic conditions (Fig. 6). The apparent K_M-value of N171D slightly decreased (Table 2) and a K_M value for N183 was only measurable under isotonic conditions (Table 2) with a similar K_M value as observed for the BGT-1 WT under hypertonic conditions in MDCK cells. Transport rates were reduced by a factor of 2 for N171D but were only slightly affected for N183D. The quantitative differences between oocytes and MDCK measurements can be attributed to the different techniques (inward current *vs* radiotracer uptake).

It can be concluded that GABA transport is only slightly affected by *N*-glycosylation in both oocytes and MDCK cells, when at least one of the two sites (N171, N183) can be glycosylated or to some extent mimicked by aspartate. In oocytes, the data suggest that the mutation of N183 does affect trafficking and thereby plasma membrane insertion (Fig. 3C), but not critically transport, when substituted by aspartate. Therefore, we investigated N183D with respect to regulatory expression and plasma membrane insertion under both isotonic and hypertonic conditions in MDCK cells (Fig. 6A, B). The amount of expressed and hence

plasma membrane inserted N183D is not up-regulated, but instead strongly down-regulated under hypertonic conditions (Fig. 6A,B, Hyp). In contrast, both *N*-glycosylated BGT-1-WT and N171D show strong up-regulation of plasma membrane insertion (Figs. 4C,D, Hyp; 6C, D). The amount of plasma membrane inserted N183D is significantly reduced under hypertonic conditions compared to isotonic conditions (Fig. 6A, B) indicating that this site has an important role in the regulation mechanism in MDCK cells. The pronounced change in plasma membrane abundance of N183D indicates furthermore that the association of *N*-glycans with N171 in EL2 is a regulatory parameter during both trafficking and plasma membrane insertion, respectively.

DISCUSSION

N-glycosylation is a sophisticated modification of protein structures by which cells control dynamics in conformational space. Domains can be stabilized after translation and during trafficking to fulfil specific requirements of their target locations.

The role of *N*-glycosylation on trafficking and transport was already described for other SLC6 transporters, too. However, the emerging picture is not entirely conclusive. Loss of *N*-glycans affected trafficking and plasma membrane insertion differently and in some cases decreases the substrate affinity [25-28, 30]. A deficiency in *N*-glycan association to the conserved site 3 was reported to reduce uptake rates in the NSS transporters GAT1 [27], CRT [25], NET [28] and SERT [30], which was mainly attributed to a reduction of inserted protein into the plasma membrane. On the other hand, the lack of *N*-glycans at site 5 has been shown to affect protein stability in DAT and GAT1 [26, 27]. In a structural context these data confirm that the architecture of EL2 in SLC6 transporters is crucial for proper targeting and substrate binding.

The situation in BGT-1 is more complex as we draw now a link between *N*-glycosylation and regulated plasma membrane insertion upon osmotic shock. The mutagenesis data point to a regulatory role of the external loop EL2 involving changes in its conformation and thereby affecting insertion and transport of BGT-1. The most surprising result of our study was the exclusive role of N183 in EL2 for regulated insertion and depletion (Fig. 6A,B, Hyp; Fig. 4E). We propose three steps in BGT-1 regulation via *N*-glycosylation: first, plasma membrane insertion and depletion as a function of the amount of added *N*-glycans; second, increased substrate affinity; and a third regulated post-translational modification upon osmotic upshift. In the following we will discuss each step in the light of the obtained mutagenesis data and conformational changes in EL2 in the presence and absence of associated *N*-glycans.

Substitution of asparagine by aspartate for both *N*-glycosylation sites individually affected only trafficking (Fig. 3C), but not transport properties of BGT-1. As a matter of fact, the double mutant did not show any measurable currents. However, this does not automatically mean that the double mutant is inactive, in fact when NN171/183DD was expressed in *Pichia pastoris* cells, it facilitated significant uptake of radioactive labelled GABA (data not shown). It might very well be that the stoichiometry of transport was altered in a way that no currents could be detected by two-electrode voltage clamp. Anyway, we conclude that both plasma membrane insertion as well as transport properties are affected when both sites are replaced by aspartate. However, introduced charges at these sites mimic the effect of *N*-glycosylation to some extent. There are several charged residues in EL2, which could provide the possibility for salt bridges and ionic interactions. The individually introduced aspartates result in mutants that show comparable substrate transport and affinity to BGT-1-WT and the amounts of *N*-glycans associated is not strongly affected, when one site is missing (Table 1). The presence of aspartate at N183 might alter the conformation of EL2 in a way that *N*-glycans can still attach to N171, while this site is not fully accessible when N183 is substituted to valine (Fig. 3A). Substitution by neutral amino acids had dramatic effects on transport and affinity (Table 1). One could assume that the association of *N*-glycans, bulky by nature, with EL2, influences the conformation and the flexibility of the loop. In return it can

be assumed that the flexibility of the loop itself is a parameter in conformational cycling during transport. In fact, EL2 is located close to the scaffold-bundle interface and also to the vestibule leading to the substrate-binding site (Figure 1B). The presence of bulky *N*-glycans could therefore block the passage of the substrate or shift the alternating-access equilibrium by populating one conformation more than the other or even by controlling the rate of the conformational change. The decrease in transport rate observed in this study when one of the *N*-glycosylation sites was substituted by alanine or valine could be explained by a change in the conformation of EL2 upon mutation, to one that is not suitable for transport. Similarly, introducing an aspartate at the conserved position 171 could lead to a conformation of EL2 that is more favourable for transport, yielding a mutant with five times higher apparent substrate affinity (Table 1, N171D).

That the architecture of EL2 could be modified by post-translational modifications such as *N*-glycosylation, or mutations is consistent with earlier observations. For example, the structure of dmDAT reveals a disulphide bond in EL2, formed by cys residues that are conserved in most of the transporters in this subfamily (hBGT1, GAT1-3, TauT, DAT and even SERT). In the case of SERT, the disulphide bond formation is crucial for obtaining a functional conformation of EL2 [43]. In the case of human DAT, the conformational state of the entire transporter can be governed by the coordination of a zinc ion to EL2 [44]. Moreover, the model of BGT-1 shows a putative interaction of EL2 with other extracellular loops, e.g., with EL4 (Figure 1C), which is known to play a key role in conformational changes in the SLC6 family [45]. Specifically, EL4 was shown to be part of an extracellular gate involved in the conformational change from outside to inside open conformation, as well as being part of the extracellular vestibule that accommodates the inhibitors [46-50]. All together we conclude that for substrate transport mediated by BGT-1 the presence of *N*-glycans at either site is not essential as long as EL2 can adopt a certain conformation.

The situation is changed when it comes to the regulatory plasma membrane insertion during hypertonic stress. Here the regulatory properties strongly depends on mature *N*-glycosylation at N183 and cannot be compensated by an introduced charged residue at N183 or even by *N*-glycans at the remaining N171 (Fig. 6).

Homology modelling of BGT-1 suggests that N183 is located in the middle of a random-coil segment (most probably a relatively flexible region), and is clearly involved in regulation (Fig. 1B,C), whereas the more conserved site 3, N171, located close to a helical segment and presumed to be a less flexible region, appears primarily to be important for substrate affinity in BGT-1. The number of *N*-glycans associated at this site might even trigger regulated insertion. We base this assumption on the fact that in oocytes, BGT-1 insertion is not regulated under hyperosmotic conditions (Fig. 2B) and we detect only a small amount of *N*-glycans linked to BGT-1 (Fig 2D, Fig. 3A), whereas in MDCK cells, in which plasma membrane insertion is regulated, the association with *N*-glycans appears to be more complex, resulting in an additional mass of ~35 kDa (Fig. 4A).

It is interesting to note that within the SLC6 family BGT-1 has evolved an EL2 sequence quite distinct from other family members (Fig. 1A). However, the mechanism of osmotic stress dependent plasma membrane insertion is not only observed in BGT-1. Kempson et *al.* identified the amino acid transport system A [51] and Yorek et *al*. the *myo*-inositol transporter SMIT [52] as being regulated under hypertonic conditions in MDCK and TALH cells, respectively. System A transport activity is increased immediately after switching MDCK cells to hypertonic medium whereas activation response of BGT-1 occurs after 24 hours and coincide with down-regulation of system A [51]. SMIT shows a comparable regulatory time pattern to BGT-1. The amount of both transporters on the plasma membrane is increased after exposing the cells to hypertonic medium and they are both depleted from the plasma membrane under isotonic conditions.

Both transporters share the same overall LeuT-like fold. In contrast to BGT-1, SMIT is predicted to have fourteen transmembrane domains [53] with a large, highly charged C-terminal domain located in the cytoplasm [54].

Interestingly, Asp-linked *N*-glycosylation sites are located in the third extracellular loop (EL3) of SMIT, which due to the topology shift of one TM helix occurring between SLC5 and SLC6 family would correspond exactly to EL2 in BGT-1. However, to date no data are available concerning *N*-glycosylation of SMIT1, except PNGase F assays for SMIT2, a sodium-coupled *myo*-inositol transporter mainly found in the cortex [55]. Latter showed no reduction in molecular weight upon PNGase F treatment suggesting that SMIT2 does not bind *N*-glycans [55]. We suggest that *N*-glycosylation might be a regulatory parameter during trafficking under hypertonic conditions for both transporters.

It is now an intriguing question if other SLC6/5 transporters also exploit *N*-glycosylation in EL2 for some sort of regulation. The very distinctive role of *N*-glycosylation in BGT-1 might draw attention to the non-conserved regions in EL2 initiating more detailed investigations into this direction of these medical important transporters in future.

ACKNOLEDGMENTS

We thank Manuel Palacín and Baruch Kanner for suggestions and experimental advice, Caroline Koshy, Stefan Köster, Sabrina Schulze, Javier Carrera-Casanova and Ahmad Reza Mehdipour for helpful discussions.

FOOTNOTES

* This work was supported by the DFG ZI-5-2 (German Research Foundation) and Collaborative Research Center 807 "Transport and Communication across Biological Membranes" (to LRF and CZ), and by the Intramural Research Program of the NIH, NINDS.

[1]The abbreviations used are: BGT-1, betaine/GABA transporter 1; BCCT, betaine carnitine choline transporter; EGFP, enhanced green fluorescent protein; GABA, γ-aminobutyric acid; MDCK, Madin-Darby canine kidney; NSS, neurotransmitter:sodium symporter; PNGase F, Peptide-N^4-(*N*-acetyl-/3-glucosaminyl)asparagine amidase F; SLC6, sodium- and chloride-dependent neurotransmitter transporter family

[2]Author contributions: ES performed all experiments with the exception of the thin sectioning, which were carried out by Friederike Joos and the two electrode voltage clamp performed by BB; CFF and CK carried out computational work; LRF supervised computational work; SAK supervised MDCK measurements; CZ designed research; CZ and ES analysed data; CZ and ES wrote the manuscript, and all authors commented on the manuscript.

REFERENCES

1 Burg, M. B. (1995) Molecular basis of osmotic regulation. Am J Physiol Renal Physiol. **268**, F983-996

2 Kwon, H. M. and Handler, J. S. (1995) Cell volume regulated transporters of compatible osmolytes. Curr Opin Cell Biol. **7**, 465-471
3 Beck, F. X., Burger-Kentischer, A. and Muller, E. (1998) Cellular response to osmotic stress in the renal medulla. Pflügers Arch. **436**, 814-827
4 Bourque, C. W. (2008) Central mechanisms of osmosensation and systemic osmoregulation. Nat Rev Neurosci. **9**, 519-531
5 Haussinger, D. (1996) The role of cellular hydration in the regulation of cell function. Biochemical Journal. **313**, 697-710
6 Reinehr, R. and Haussinger, D. (2006) Hyperosmotic activation of the CD95 death receptor system. Acta Physiol. **187**, 199-203
7 Dmitrieva, N. I. and Burg, M. B. (2005) Hypertonic stress response. Mutat Res-Fund Mol M. **569**, 65-74
8 Nakayama, Y., Peng, T., Sands, J. M. and Bagnasco, S. M. (2000) The TonE/TonEBP pathway mediates tonicity-responsive regulation of UT-A urea transporter expression. J Biol Chem. **275**, 38275-38280
9 Holthauzen, L. M. F. and Bolen, D. W. (2007) Mixed osmolytes: The degree to which one osmolyte affects the protein stabilizing ability of another. Prot Sci. **16**, 293-298
10 Broer, S. and Gether, U. (2012) The Solute Carrier Family 6. Br J Pharmacol. **167**, 256-278
11 Kempson, S. A. and Montrose, M. H. (2004) Osmotic regulation of renal betaine transport: transcription and beyond. Pflügers Arch-Eur J Physiol. **449**, 227-234
12 Zhou, Y., Holmseth, S., Hua, R., Lehre, A. C., Olofsson, A. M., Poblete-Naredo, I., Kempson, S. A. and Danbolt, N. C. (2012) The betaine-GABA transporter (BGT1, slc6a12) is predominantly expressed in the liver and at lower levels in the kidneys and at the brain surface. Am J Physiol Renal Physiol. **302**, F316-328
13 Rasola, A., Galietta, L. J., Barone, V., Romeo, G. and Bagnasco, S. (1995) Molecular cloning and functional characterization of a GABA/betaine transporter from human kidney. FEBS Lett. **373**, 229-233
14 Matskevitch, I., Wagner, C. A., Stegen, C., Broer, S., Noll, B., Risler, T., Kwon, H. M., Handler, J. S., Waldegger, S., Busch, A. E. and Lang, F. (1999) Functional characterization of the Betaine/gamma-aminobutyric acid transporter BGT-1 expressed in Xenopus oocytes. J Biol Chem. **274**, 16709-16716
15 Lever, M., Sizeland, P. C., Frampton, C. M. and Chambers, S. T. (2004) Short and long-term variation of plasma glycine betaine concentrations in humans. Clin Biochem. **37**, 184-190
16 Laryea, M. D., Steinhagen, F., Pawliczek, S. and Wendel, U. (1998) Simple method for the routine determination of betaine and N,N-dimethylglycine in blood and urine. Clin Chem. **44**, 1937-1941
17 Uchida, S., Yamauchi, A., Preston, A. S., Kwon, H. M. and Handler, J. S. (1993) Medium tonicity regulates expression of the Na(+)- and Cl(-)-dependent betaine transporter in Madin-Darby canine kidney cells by increasing transcription of the transporter gene. J Clin Invest. **91**, 1604-1607
18 Kwon, H. M., Yamauchi, A., Uchida, S., Preston, A. S., Garcia-Perez, A., Burg, M. B. and Handler, J. S. (1992) Cloning of the cDNA for a Na+/myo-inositol cotransporter, a hypertonicity stress protein. J Biol Chem. **267**, 6297-6301
19 Miyakawa, H., Woo, S. K., Dahl, S. C., Handler, J. S. and Kwon, H. M. (1999) Tonicity-responsive enhancer binding protein, a rel-like protein that stimulates transcription in response to hypertonicity. Proc Natl Acad Sci U S A. **96**, 2538-2542
20 Takenaka, M., Preston, A. S., Kwon, H. M. and Handler, J. S. (1994) The tonicity-sensitive element that mediates increased transcription of the betaine transporter gene in response to hypertonic stress. J Biol Chem. **269**, 29379-29381
21 Ito, T., Fujio, Y., Hirata, M., Takatani, T., Matsuda, T., Muraoka, S., Takahashi, K. and Azuma, J. (2004) Expression of taurine transporter is regulated through the TonE

(tonicity-responsive element)/TonEBP (TonE-binding protein) pathway and contributes to cytoprotection in HepG2 cells. Biochem J. **382**, 177-182

22 Klaus, F., Palmada, M., Lindner, R., Laufer, J., Jeyaraj, S., Lang, F. and Boehmer, C. (2008) Up-regulation of hypertonicity-activated myo-inositol transporter SMIT1 by the cell volume-sensitive protein kinase SGK1. The Journal of physiology. **586**, 1539-1547

23 Lis, H. and Sharon, N. (1993) Protein glycosylation. Structural and functional aspects. Eur J Biochem. **218**, 1-27

24 Kukuruzinska, M. A. and Lennon, K. (1998) Protein N-glycosylation: molecular genetics and functional significance. Crit Rev Oral Biol Med. **9**, 415-448

25 Straumann, N., Wind, A., Leuenberger, T. and Wallimann, T. (2006) Effects of N-linked glycosylation on the creatine transporter. Biochem J. **393**, 459-469

26 Li, L. B., Chen, N., Ramamoorthy, S., Chi, L., Cui, X. N., Wang, L. C. and Reith, M. E. (2004) The role of N-glycosylation in function and surface trafficking of the human dopamine transporter. J Biol Chem. **279**, 21012-21020

27 Cai, G., Salonikidis, P. S., Fei, J., Schwarz, W., Schulein, R., Reutter, W. and Fan, H. (2005) The role of N-glycosylation in the stability, trafficking and GABA-uptake of GABA-transporter 1. Terminal N-glycans facilitate efficient GABA-uptake activity of the GABA transporter. FEBS J. **272**, 1625-1638

28 Nguyen, T. T. and Amara, S. G. (1996) N-linked oligosaccharides are required for cell surface expression of the norepinephrine transporter but do not influence substrate or inhibitor recognition. J Neurochem. **67**, 645-655

29 Melikian, H. E., Ramamoorthy, S., Tate, C. G. and Blakely, R. D. (1996) Inability to N-glycosylate the human norepinephrine transporter reduces protein stability, surface trafficking, and transport activity but not ligand recognition. Mol Pharmacol. **50**, 266-276

30 Tate, C. G. and Blakely, R. D. (1994) The effect of N-linked glycosylation on activity of the Na(+)- and Cl(-)-dependent serotonin transporter expressed using recombinant baculovirus in insect cells. J Biol Chem. **269**, 26303-26310

31 Forrest, L. R., Kramer, R. and Ziegler, C. (2011) The structural basis of secondary active transport mechanisms. Biochim Biophys Acta. **1807**, 167-188

32 Broer, S. (2010) Xenopus laevis Oocytes. Methods Mol Biol. **637**, 295-310

33 Jack, D. L., Paulsen, I. T. and Saier, M. H. (2000) The amino acid/polyamine/organocation (APC) superfamily of transporters specific for amino acids, polyamines and organocations. Microbiology. **146 (Pt 8)**, 1797-1814

34 Haase, W. and Koepsell, H. (1989) Electron microscopic immunohistochemical localization of components of Na+-cotransporters along the rat nephron. Eur J Cell Biol. **48**, 360-374

35 Lörinczi, E., Tsivkovskii, R., Haase, W., Bamberg, E., Lutsenko, S. and Friedrich, T. (2008) Delivery of the Cu-transporting ATPase ATP7B to the plasma membrane in Xenopus oocytes. Biochim Biophys Acta. **1778**, 896-906

36 Kempson, S. A., Parikh, V., Xi, L., Chu, S. and Montrose, M. H. (2003) Subcellular redistribution of the renal betaine transporter during hypertonic stress. Am J Physiol Cell Physiol. **285**, C1091-1100

37 Forrest, L. R. and Rudnick, G. (2009) The rocking bundle: a mechanism for ion-coupled solute flux by symmetrical transporters. Physiology (Bethesda, Md.). **24**, 377-386

38 Motulsky, H. (1999) Analyzing Data with GraphPad Prism. GraphPad Software Inc., San Diego, CA, USA.

39 Notredame, C., Higgins, D. G. and Heringa, J. (2000) T-Coffee: A novel method for fast and accurate multiple sequence alignment. J Mol Biol. **302**, 205-217

40 Sali, A. and Blundell, T. L. (1993) Comparative protein modelling by satisfaction of spatial restraints. J Mol Biol. **234**, 779-815

41 Laskowski, R. A., MacArthur, M. W., Moss, D. S. and Thornton, J. M. (1993) PROCHECK: a program to check the stereochemical quality of protein structures. Journal of Applied Crystallography. **26**, 283-291
42 Penmatsa, A., Wang, K. H. and Gouaux, E. (2013) X-ray structure of dopamine transporter elucidates antidepressant mechanism. Nature. **503**, 85-90
43 Chen, J. G., Liu-Chen, S. and Rudnick, G. (1997) External cysteine residues in the serotonin transporter. Biochemistry. **36**, 1479-1486
44 Loland, C. J., Norgaard-Nielsen, K. and Gether, U. (2003) Probing dopamine transporter structure and function by Zn2+-site engineering. Eur J Pharmacol. **479**, 187-197
45 Krishnamurthy, H., Piscitelli, C. L. and Gouaux, E. (2009) Unlocking the molecular secrets of sodium-coupled transporters. Nature. **459**, 347-355
46 Mitchell, S. M., Lee, E., Garcia, M. L. and Stephan, M. M. (2004) Structure and function of extracellular loop 4 of the serotonin transporter as revealed by cysteine-scanning mutagenesis. J Biol Chem. **279**, 24089-24099
47 Stephan, M. M., Chen, M. A., Penado, K. M. and Rudnick, G. (1997) An extracellular loop region of the serotonin transporter may be involved in the translocation mechanism. Biochemistry. **36**, 1322-1328
48 Smicun, Y., Campbell, S. D., Chen, M. A., Gu, H. and Rudnick, G. (1999) The role of external loop regions in serotonin transport. Loop scanning mutagenesis of the serotonin transporter external domain. J Biol Chem. **274**, 36058-36064
49 Focke, P. J., Wang, X. and Larsson, H. P. (2013) Neurotransmitter transporters: structure meets function. Structure (London, England : 1993). **21**, 694-705
50 Yamashita, A., Singh, S. K., Kawate, T., Jin, Y. and Gouaux, E. (2005) Crystal structure of a bacterial homologue of Na+/Cl--dependent neurotransmitter transporters. Nature. **437**, 215-223
51 Kempson, S. A. (1998) Differential activation of system A and betaine/GABA transport in MDCK cell membranes by hypertonic stress. Biochim Biophys Acta. **1372**, 117-123
52 Yorek, M. A., Dunlap, J. A. and Lowe, W. L., Jr. (1999) Osmotic regulation of the Na+/myo-inositol cotransporter and postinduction normalization. Kidney Int. **55**, 215-224
53 Turk, E. and Wright, E. M. (1997) Membrane topology motifs in the SGLT cotransporter family. J Membr Biol. **159**, 1-20
54 Hein, S., Prassolov, V., Zhang, Y., Ivanov, D., Lohler, J., Ross, S. R. and Stocking, C. (2003) Sodium-dependent myo-inositol transporter 1 is a cellular receptor for Mus cervicolor M813 murine leukemia virus. Journal of virology. **77**, 5926-5932
55 Lahjouji, K., Aouameur, R., Bissonnette, P., Coady, M. J., Bichet, D. G. and Lapointe, J. Y. (2007) Expression and functionality of the Na+/myo-inositol cotransporter SMIT2 in rabbit kidney. Biochim Biophys Acta. **1768**, 1154-1159

FIGURE LEGENDS

FIGURE 1. Sequence alignment and homology model of the NSS family transporter BGT-1. (**A**) Sequence alignment of representative NSS family members (human BGT1, SLC6A12, P48065; dog BGT1, SLC6A12, P27799; human GAT2, SLC6A13, Q9NSD5; human GAT3, SLC6A11, P48066; human GAT1, SLC6A1, P30531; human TauT, SLC6A6, P31641; human DAT, SLC6A3, Q01959; and *Drosophila melanogaster* DAT, PDB entry 4M48:A, which is truncated at residues 164-206 compared to SLC6A6, at the position indicated by *) with varying numbers of *N*-glycosylation sites in EL2. Six *N*-glycosylation sites are found in total, and are labelled 1-6 (red rectangles and bars). Conserved residues are coloured with increasingly dark blue backgrounds. (**B, C**) Homology model of BGT-1 based

on dmDAT (PDB entry 4M48), shown as cartoons and viewed from the plane of the membrane, for (**B**) the whole protein, and (**C**) a close-up of the extracellular surface. Helices in the four-helix bundle containing transmembrane helices 1, 2, 6, and 7 are colored pink, while the transmembrane helices in the so-called scaffold are colored dark blue. Loops EL2 and EL4 are shown in orange and cyan, respectively. The segment of EL2 with the lowest confidence due to the lack of template during the modelling process is highlighted in yellow. Two sodium ions, one chloride ion and a GABA molecule are shown in the central binding sites as spheres (purple and green for sodium and chloride, respectively). The disulphide bridge formed by residues C157 and C166 is shown as orange sticks. The glycosylation sites N171 and N183 are shown as red sticks, while V188 and I365 are shown as orange and cyan sticks respectively.

FIGURE 2. Response of BGT-1 to GABA in the presence of hypertonic conditions and membrane distribution of *N*-glycosylated and de-glycosylated BGT-1 in *Xenopus* oocytes. (**A**, **B**) Traces represent typical records as obtained using 7 oocytes from 2 different frogs. Oocytes were either injected with water (**A**) or BGT-1 RNA (**B**), clamped at a potential of -60 mV, and superfused with 10 mM GABA dissolved in ORi (black bar, 10 mM GABA). Hypertonic conditions were achieved by adding 220 mM sucrose to ORi (black bar, + 220 mM Sucrose) after which the effect of betaine (black bar, 10 mM GABA) was tested again. Under isotonic conditions, GABA only induced currents in the *bgt1*-expressing oocytes, specifically inward currents of -36.5±13.8 nA (**B**). Hypertonic conditions led to inward currents in both water-injected- (**A**) and BGT-1-RNA-injected oocytes (**B**), but GABA-mediated currents in *bgt1*-expressing oocytes were reduced under hypertonic conditions (-28.5±26.8 nA) in comparison to isotonic conditions. (**C, D**) Fractionation of oocyte membranes (80 oocytes of WT and 100 oocytes of WT^{+P}) showing a distribution of (**C**) WT and (**D**) WT^{+P} in the plasma membrane (PM), in the rough Endoplasmic Reticulum (rER), and in the trans-Golgi network (TGN) of oocytes.

FIGURE 3. Expression and distribution of BGT-1 and *N*-glycosylation site mutants in oocytes. (**A**) Western blot against BGT-1 specific antibody for oocyte membranes containing mutants treated with (+) and without PNGase F. Treatment of oocytes with PNGase F resulted in a 70 kDa glycosylated form (WT) and a 60 kDa deglycosylated isoform (WT, +). N171D treated with PNGase F (N171D, +) shows a shift similar to that observed for WT BGT-1, with a prominent band at 60 kDa. N183D shows a dramatically reduced amount of the glycosylated form at 70 kDa, but dominantly the un-glycosylated form at 60 kDa (N183D, +). NN171/183DD is detected at 60 kDa both with and without PNGase F (NNDD, +). N171A and N171V are still glycosylated before PNGase F, demonstrated by a band shift after PNGase F treatment. However, the extent of *N*-glycosylation is lower than for WT and N171D. The N183V mutant shows no shift upon PNGase F treatment, similar to the double mutant NN171/183DD. An exemplary Western blot is shown of three replicates. (**B**) Fractionation of oocyte membranes (150 oocytes of NN171/183D) showing the distribution of NN171/183DD in the plasma membrane (PM), in the rough Endoplasmic Reticulum (rER), and in the trans-Golgi network (TGN), where the latter shows minor degradation (arrow). An exemplary Western blot is shown of three replicates. (**C**) Immunogold-labelling of thin-sectioned oocytes containing WT, N171D, N183D and NN171/183DD reveal the abundance

of the WT in the plasma membrane, whereas N171D and N183D are less abundant in the plasma membrane, and NN171/183DD is detected only in smaller amounts in the plasma membrane and stays mainly intracellular, in the rER. Micrographs are representative of a series of 20 identical experiments each (WT: 30 ± 5 gold-labeled BGT-1 molecules in a comparable section, N171D: 21 ± 3, N183D: 15 ± 2, NN171/183DD: 9 ± 1).

FIGURE 4. Membrane distribution of de-glycosylated BGT-1 in MDCK cells. (**A**) Western blot analysis of endogenous BGT-1 (WT_{end}) before and after treatment with PNGase F (WT_{end}^{+P}) using a BGT-1 specific antibody reveal a band shift from 95 kDa (WT_{end}) to 55 kDa (WT_{end}^{+P}). An exemplary Western blot is shown of three replicates. (**B**) Western blot of MDCK membranes expressing EGFP-BGT-1-WT using a GFP-tag reveals a fully glycosylated form of the BGT-1-WT at 120 kDa accounting for the 27 kDa EGFP-tag (WT_{EGFP}) and a 95 kDa band of EGFP-BGT-1-WT after PNGase F treatment (WT_{EGFP}^{+P}). An exemplary Western blot is shown of three replicates. (**C**) EGFP-BGT-1-WT exposed to iso- (Iso) and hypertonic (Hyp) growth medium resulting in an increase of protein at the plasma membrane during hypertonicity. An exemplary Western blot is shown of three replicates. (**D**) Fluorescence microscopy of MDCK cells under iso- (Iso) and hypertonic (Hyp) conditions (24 hours) expressing BGT-1-WT_{EGFP} demonstrates a clear subcellular distribution to the plasma membrane under hypertonicity. The same hypertonic conditions and treatment with PNGase F for 6 hours (Hyp^{+P}) result in a partial redistribution of BGT-1-WT. (**E**) Distribution of both EGFP-BGT-1-WT and EGFP-BGT-1-WT treated with PNGase F for 6 hours in MDCK cells after 24 hours in hypertonic medium and then switched to fresh isotonic growth medium for further 24 hours ($Hyp_{recovery}$, $Hyp^{+P}_{recovery}$). (Scale bar (**D**, **E**): 20 µm)

FIGURE 5. Activity of glycosylated BGT-1 and de-glycosylated BGT-1 in MDCK cells. K_M-values of endogenous BGT-1 (filled circles) and de-glycosylated BGT-1 after PNGase F treatment (open squares) were obtained from the uptake rates of [^{3}H]GABA in pmol per mg per min in MDCK cells. Each point shows the average of at least three independent experiments. The error bars represent a mean ±SD of three independent measurements. *$P <$ 0.001, compared with controls (ANOVA).

FIGURE 6. **Expression and distribution of N171D and N183D under iso- and hypertonic conditions in MDCK cells**. (**A, B**) Western blot analysis and fluorescence microscopy of N183D under iso- (Iso) and hypertonic (Hyp) conditions show a decrease in its expression during hypertonic growth conditions. Under isotonic conditions (Iso) N183D is located in the plasma membrane and intracellular whereas under hypertonic conditions (Hyp) the overall amount is strongly reduced. An exemplary Western blot is shown of three replicates. (**C, D**) Western blot analysis and fluorescence microscopy of N171D under iso- (Iso) and hypertonic (Hyp) conditions show an increase in its expression during hypertonic growth conditions. Under isotonic conditions (Iso) N171D is primary located intracellular whereas under hypertonic conditions (Hyp) the mutant is found in the plasma membrane similar to EGFP-BGT1. (Scale bar: 20 µm). An exemplary Western blot is shown of three replicates.

823

TABLE 1. Functional analysis of glycosylated, de-glycosylated and mutants of BGT-1 in *Xenopus* oocytes.

K_M-values and ΔI_{max} of BGT-1 wildtype (WT) expressed in *Xenopus* oocytes with and without treatment of tunicamycin ($^{+Tun}$) and PNGase F ($^{+P}$) as well as K_M-values for the single mutants (N171D, N171V, N171A, N183D, N183V) without treatment of tunicamycin and PNGase F for GABA are listed. For the double mutant (NN171/183DD) because of the low currents no K_M could be determined. Significantly different from WT controls ($P < 0.05$).

Values were determined in at least three independent observations.

	$K_{M,\ -60\ mV}$ [μM]	$\Delta I_{max,\ -60\ mV}$ [nA]
WT	11.7 ± 0.4	- 47.0 ± 9.5
WT $^{+P}$	29.4 ± 7.5	- 16.6 ± 2.2
WT $^{+Tun}$	209.0 ± 80	- 10.0 ± 1.9
N171D	2.1 ± 0.5	- 13.6 ± 1.1
N171V	3200 ± 600	- 10.2 ± 2.4
N171A	> 5000	- 6.5 ± 5.5
N183D	9.5 ± 1.2	- 21.1 ± 0.7
N183V	>5000	-8.2 ± 1.6
NN171/183DD	BD*	BD*

* Below detection (BD) limit

TABLE 2. Functional characterization of glycosylated, de-glycosylated and mutants of BGT-1 in MDCK and HEK cells.

K_M-values and V_{max} of endogenous BGT-1with and without treatment of PNGase F ($^{+P}$) under hypertonic conditions for 24 h in MDCK cells. Both, N171D and N183D were analysed in HEK cells and N183D under isotonic conditions. Significantly different from WT controls ($P < 0.001$).

Each value represents the average ± s.d. of three independent measurements.

	K_M (μM)	V_{max} (pmol/mg/min)
BGT-1-WT	41.6 ± 23.7	0.0159 ± 0.003
BGT-1-WT^{+P}	50.2 ± 16.4	0.0109 ± 0.001
N171D	30.4 ± 14.6	0.0070 ± 0.004
N183D$_{iso}$	45.4 ± 12.2	0.0106 ± 0.003

848

849 FIGURE 1.

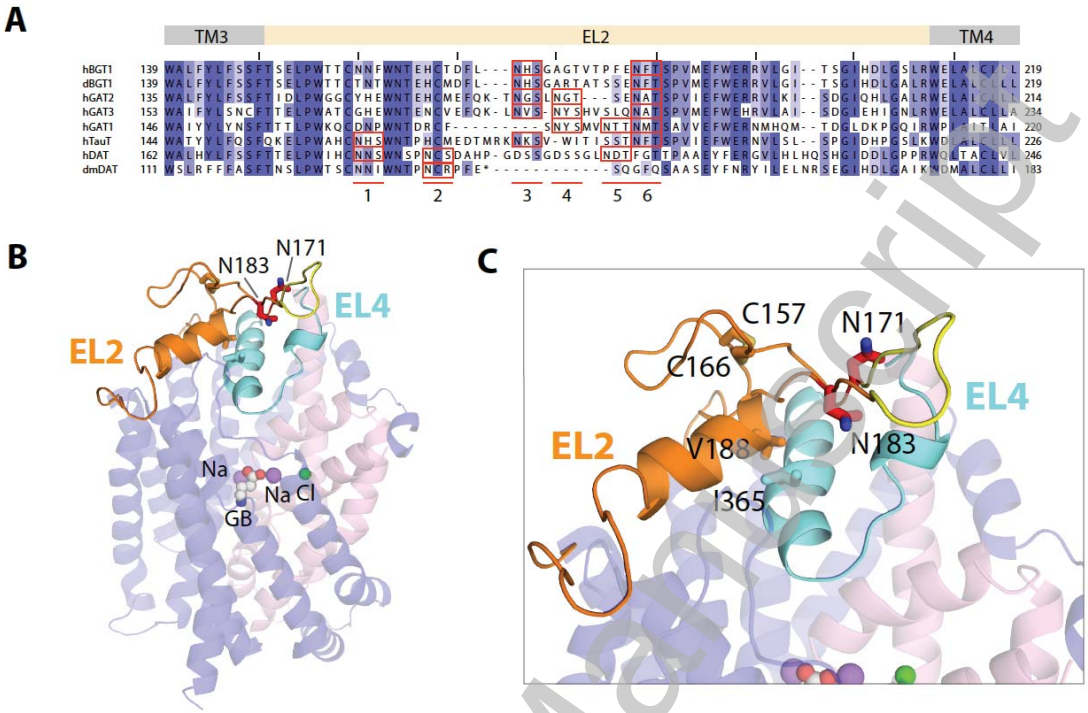

850

851

852

853

854 FIGURE 2.

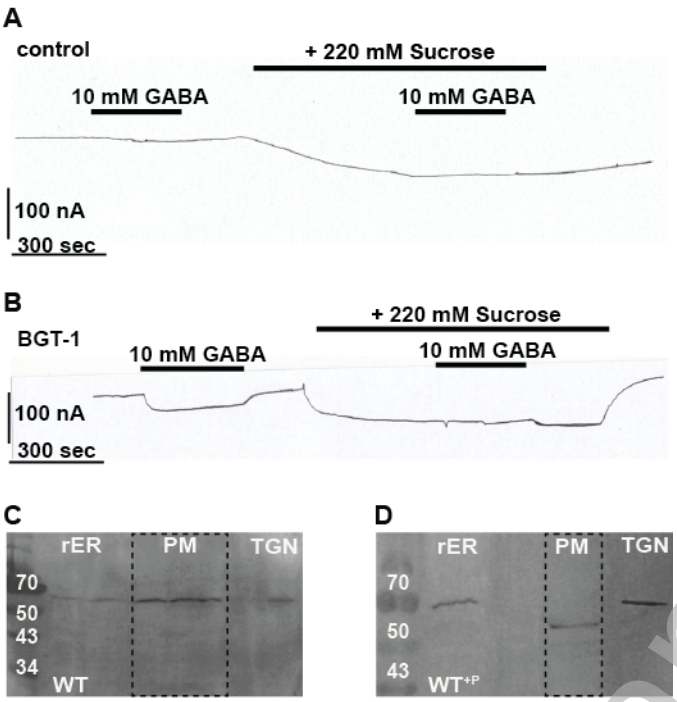

855

856

857

858

859 FIGURE 3.

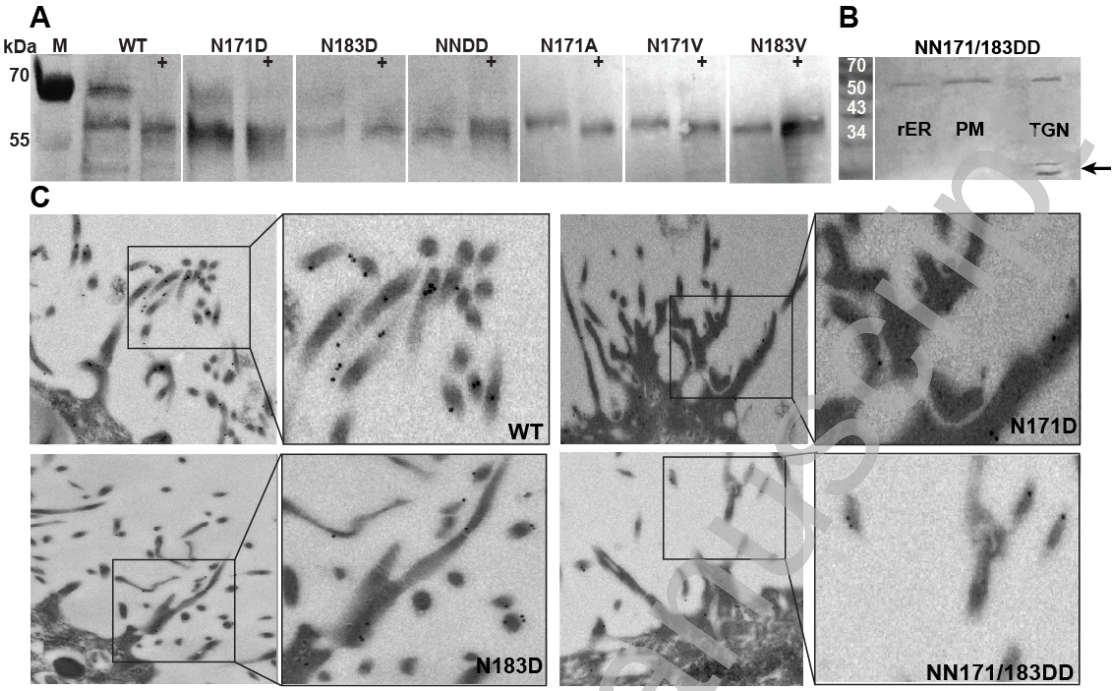

860

861

862

863

864 FIGURE 4.

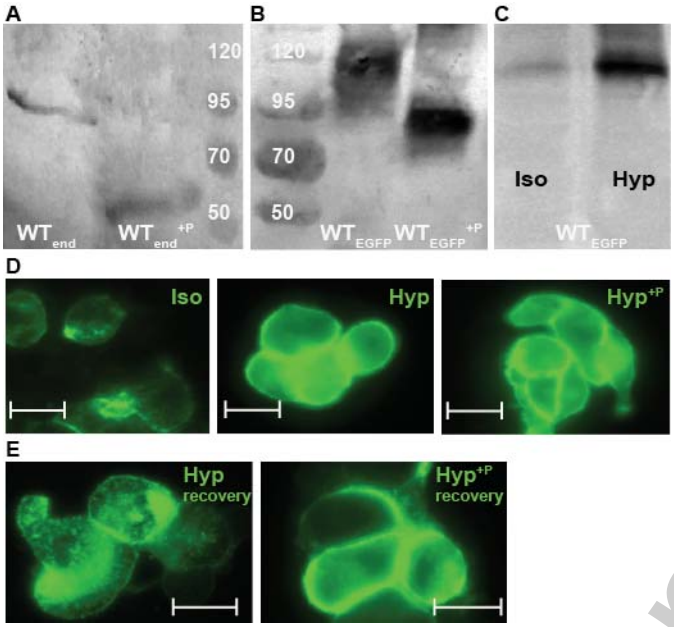

865

866

867

868

869 FIGURE 5.

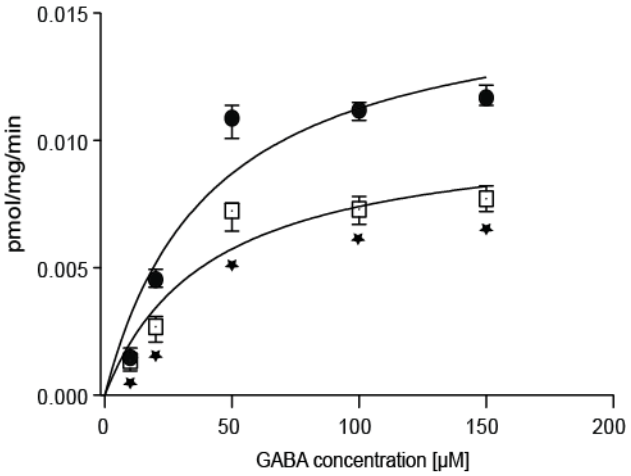

870

871

872

873

874 FIGURE 6.

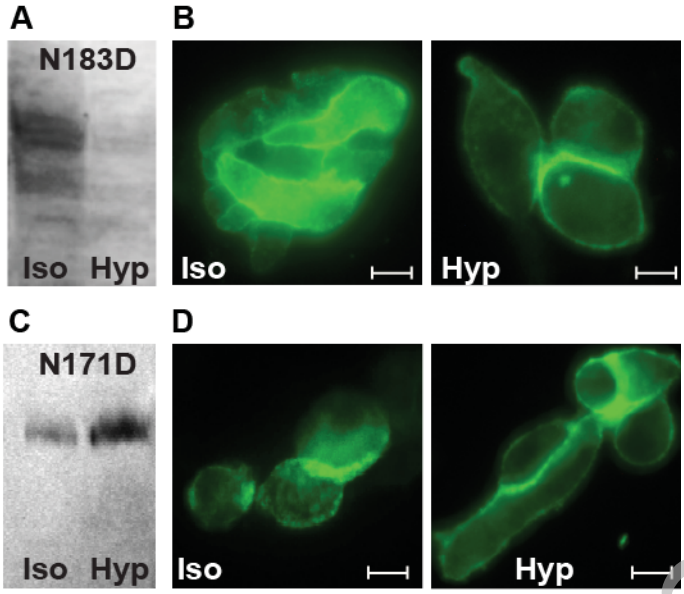

875